RSC Advances

PAPER

View Article Online
View Journal | View Issue

Cite this: *RSC Adv.*, 2024, **14**, 22676

Design, synthesis, and anti-mycobacterial evaluation of 1,8-naphthyridine-3-carbonitrile analogues†

Yogesh Mahadu Khetmalis,[a] Singarapalle Shobha,[b] Adinarayana Nandikolla,[a] Ala Chandu,[c] Sankaranarayanan Murugesan,[c] Muthyala Murali Krishna Kumar[b] and Kondapalli Venkata Gowri Chandra Sekhar *[a]

Twenty-eight compounds, *viz.*, 1,8-naphthyridine-3-carbonitrile (**ANC** and **ANA**) derivatives, were designed and synthesized through a molecular hybridization approach. The structures of these compounds were analyzed and confirmed using ^{1}H NMR, ^{13}C NMR, LCMS, and elemental analyses. The synthesized compounds were evaluated by *in vitro* testing for their effectiveness against tuberculosis using the MABA assay, targeting the *Mycobacterium tuberculosis* H37Rv strain. Their minimum inhibitory concentration (MIC) was determined, showing that the tested compounds' MIC values ranged from 6.25 to ≤50 μg mL^{-1}. Among the derivatives studied, **ANA-12** demonstrated prominent anti-tuberculosis activity with a MIC of 6.25 μg mL^{-1}. Compounds **ANC-2**, **ANA-1**, **ANA 6–8**, and **ANA-10** displayed moderate to good anti-tuberculosis activity with MIC values of 12.5 μg mL^{-1}. Compounds with MIC ≤ 12.5 μg mL^{-1} were screened against human embryonic kidney cells to assess their potential cytotoxicity. Interestingly, these compounds showed less toxicity towards normal cells, with a selectivity index value ≥ 11. To further evaluate the binding pattern in the active site of enoyl-ACP reductase (InhA) from Mtb (PDB-4TZK), a molecular docking analysis of compound **ANA-12** was performed using the glide module of Schrodinger software. The stability, confirmation, and intermolecular interactions of the cocrystal ligand and the highly active compound **ANA-12** on the chosen target protein were investigated through molecular dynamics simulations lasting 100 ns. *In silico* predictions were utilized to assess the ADMET properties of the final compounds. A suitable single crystal was developed and analyzed for compound **ANA-5** to gain a deeper understanding of the compounds' structures.

Received 11th June 2024
Accepted 11th July 2024

DOI: 10.1039/d4ra04262j

rsc.li/rsc-advances

Introduction

Tuberculosis (TB), an infection caused by *Mycobacterium tuberculosis* (Mtb), has emerged as a threat to the security of global health after COVID-19, the leading cause of mortality from a single infectious agent. 10 million people were diagnosed with TB in 2020, and 1.5 million passed away, according to the World Health Organization's (WHO) TB report for 2021.[1–3] Different types of drug resistance is the major issue with the currently used anti-TB drugs. Regrettably, the emergence of drug resistance is linked to poor adherence, long duration, toxic effects, and poor efficacy of these medications.[4,5] TB is curable and treatable using a typical course of first-line anti-tubercular drugs such as isoniazid, rifampin, pyrazinamide, and ethambutol. Though second- and third line drugs are also available for treating TB-resistant patients, they still have some significant disadvantages, such as long duration of treatment, higher cost involved for prolonged treatment, and poor drug compatibility.[6,7] If the most effective first-line anti-TB drugs don't work, it leads to multidrug-resistant TB (MDR-TB), one of the most challenging origins of treating TB. As a result, the patient must move to the second-line anti-TB treatments, which combine more than five therapies and take more than a year to work. This frequently leads to medication toxicity and may even cause extensively drug-resistant tuberculosis (XDR-TB).[6–8] There is a strong need for the development of new anti-TB medications that are more effective, take less time to work, and have higher patient compliance.

According to estimates, heterocyclic compounds comprise around 62% of the active components in pharmaceuticals. There are nitrogen-containing molecules in 91% of these compounds. Nitrogen-containing heterocycles include both

[a]*Department of Chemistry, Birla Institute of Technology and Science, Pilani, Hyderabad Campus, Jawahar Nagar, Hyderabad 500 078, Telangana, India. E-mail: kvgc@hyderabad.bits-pilani.ac.in; kvgcs.bits@gmail.com; Tel: +91 40 66303527*

[b]*College of Pharmaceutical Sciences, Andhra University, Visakhapatnam, Andhra Pradesh – 530 003, India*

[c]*Medicinal Chemistry Research Laboratory, Department of Pharmacy, Birla Institute of Technology and Science, Pilani, 333031, India*

† Electronic supplementary information (ESI) available. CCDC 2342616. For ESI and crystallographic data in CIF or other electronic format see DOI: https://doi.org/10.1039/d4ra04262j

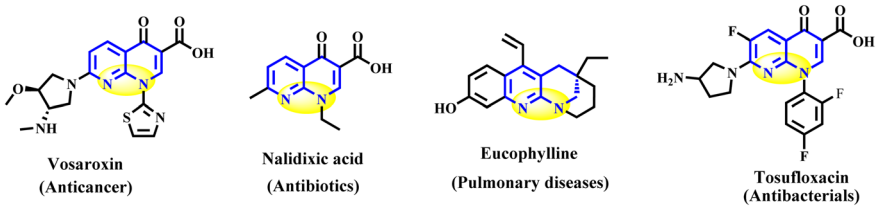

Fig. 1 Structures of commercial drugs containing a 1,8-naphthyridine nucleus.

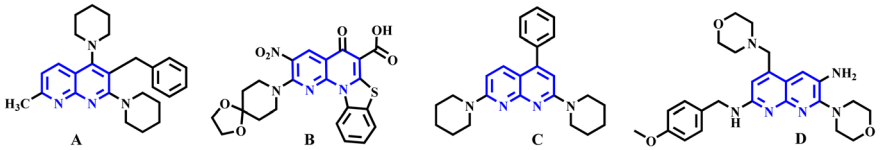

Fig. 2 Structures of anti-tubercular compounds based on 1.8-naphthyridine core.

naturally occurring 1,8-naphthyridine derivatives and those that are chemically synthesized.[9–11] The study has revealed that these 1,8-naphthyridine derivatives have a variety of biological activities, including anti-tubercular,[12] anti-bacterial,[13] antiviral,[14] anti-inflammatory,[15] and antitumor.[16] Some of the 1,8-naphthyridine-based commercial drugs currently in use are shown in Fig. 1.[17]

The anti-tubercular properties of several substituted 1,8-naphthyridine analogs are disclosed.[18–22] A group led by Badawneh and colleagues reported several 1,8-naphthyridine derivatives and tested them for anti-mycobacterial activity. Among all tested compounds, **A** is the most potent, with a 96% inhibition and standard drug rifampicin, exhibited 98% inhibition against Mtb H37Rv.[19] Murugesan and colleagues reported that naphthyridone derivatives can be used to treat multi-drug resistant TB. The most active molecule among the said compounds, **B**, has *in vitro* minimal inhibitory concentrations (MIC) of 0.19 and 0.04 μM against Mtb H37Rv and MDR-TB, respectively.[20] Furthermore, Muwaffag and the group showed 1,8-naphthyridine derivatives to have anti-tubercular activity against Mtb H37Rv. The MICs of compound **C** was 6.25 μg mL^{-1}, indicating good activity.[21] The same research group has previously reported on the anti-tubercular activity of morpholino 1,8-naphthyridine derivatives. Compound **D** showed promising anti-tubercular activity with substantial activity against Mtb H37Rv with a MIC value of 0.25 ± 0.04 μg mL^{-1} (Fig. 2).[22]

A significant functional group extensively present in both pharmacological medicines and natural compounds is the nitrile group.

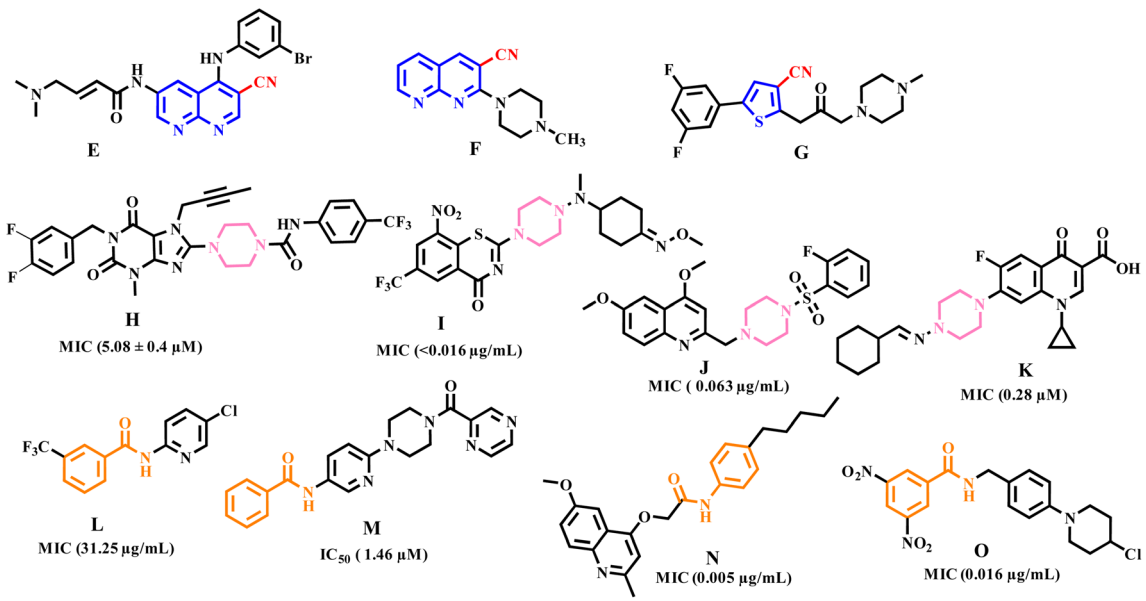

Fig. 3 Nitrile, groups containing compounds that exhibit biological activity and piperazine and benzamide-based anti-tubercular agents reported in the literature.

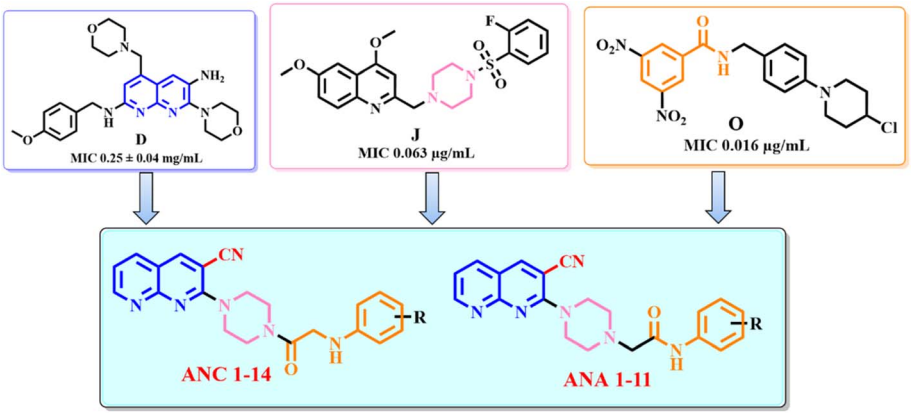

Fig. 4 Design approach for designing the target compounds.

In the past few decades, the Food and Drug Administration (FDA) has approved more than 30 nitrile-containing medicine for the therapy of a wide range of clinical problems.[23] A nitrile group can provide additional benefits including increased binding affinity to the target, improved pharmacokinetic profile of parent pharmaceuticals, and decreased drug resistance, therefore it has steadily emerged as a promising technique in rational drug design.[24] There are many groups that reported nitrile groups containing compounds as biological agents including anti-tubercular activity.[25–28] Fig. 3 shows the structures of a few nitrile groups containing compounds (**E**, **F**, **G**) that exhibit biological activity.[25,26,28] The piperazine skeleton has also been acknowledged as an effective pharmacophore against mycobacterial infections with the aforementioned advantageous characteristics.[29,30] Several piperazine-containing analogs were made and tested for their anti-TB activity with improved hydrogen bonding ability, dipole moment, stability, and stiffness under *in vivo* circumstances in the pursuit of discovering new anti-TB hybrids molecules.[30,31] Fig. 3 shows the structures of a few compounds (**H**, **I**, **J**, **K**) containing piperazine moiety that exhibit anti-TB activity.[31–34] Benzamide derivatives offer a wide spectrum of biological activities, and few researchers have made amide derivatives (**L**, **M**, **N**, **O**) as anti-TB agents. Structures of some of the anti-TB amide agents' is shown in Fig. 3.[35–38]

Molecular hybridization stands out as a widely embraced method for crafting new pharmacological frameworks. It involves amalgamating multiple components or pharmacophore units derived from familiar biological structures to design new ones. Acknowledging the importance of 1,8-naphthyridine, piperazine, and benzamide in their role as anti-tubercular agents, the present study combines these scaffolds into a unified framework. This integration lead to the design and synthesis of new anti-tubercular agents, namely **ANC 1–14** and **ANA 1–12** (Fig. 4).

Results and discussion

Chemistry

The synthetic schemes, shown in Scheme 1 and 2, has been used to synthesize the final target compounds 2-(4-(phenylglycyl) piperazin-1-yl)-1,8-naphthyridine-3-carbonitrile (**ANC 1–14**), 2-(4-(3-cyano-1,8-naphthyridin-2-yl) piperazin-1-yl)-*N*-phenylacetamide (**ANA 1–11**) and 2-(4-(5-nitrofuran-2-carbonyl) piperazin-1-yl)-1,8-naphthyridine-3-carbonitrile (**ANA-12**).

Target compounds (**ANC 1–14**) and (**ANA 1–12**) were synthesized as shown in Scheme 1 and 2. The intermediate **ANI-1** was prepared as per the literature reported protocol.[39] Compound **ANI-1** on treatment with chloroacetyl chloride in the presence of triethylamine (Et_3N) as a base at room temperature yielded **ANI-2.** Confirmation of compound **ANI-2**, is by

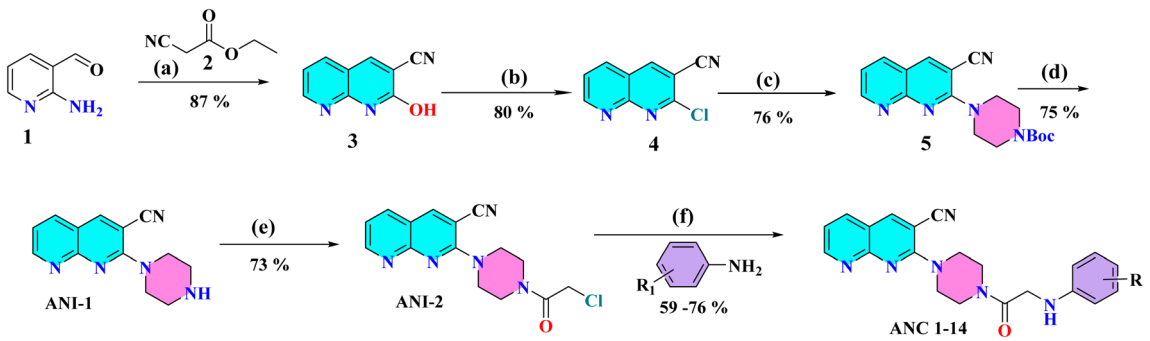

Scheme 1 Synthesis of intermediates (**ANI-1**, **ANI-2**) and 2-(4-(phenylglycyl) piperazin-1-yl)-1,8-naphthyridine-3-carbonitrile (**ANC 1–14**). Reagents and conditions (a) piperidine, grinding, 1 h, (b) $POCl_3$, *N*,*N*-dimethylaniline, 120 °C, 6 h (c) *N*-boc-piperazine, DMF, 120 °C, 4 h (d) 4.0 M HCl in dioxane, DCM, 0 °C-rt, 6 h (e) 2-chloroacetyl chloride, DCM, Et_3N, rt, 4 h (f) substituted anilines, Na_2CO_3, KI, DMF, 120 °C, 4–8 h.

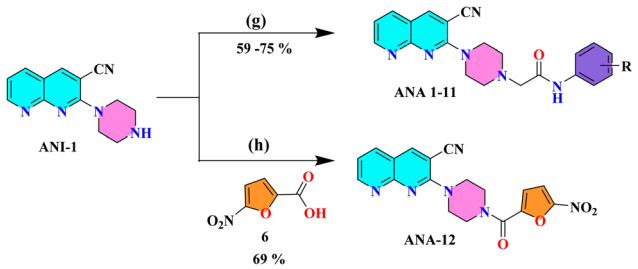

Scheme 2 Synthesis of 2-(4-(3-cyano-1,8-naphthyridin-2-yl) piperazin-1-yl)-*N*-phenylacetamide (**ANA 1–11**) derivatives and 2-(4-(5-nitrofuran-2-carbonyl) piperazin-1-yl)-1,8-naphthyridine-3-carbonitrile (**ANA-12**). Reagents and conditions (g) substituted *N*-phenylacetamides, Na_2CO_3, KI, DMF, 120 °C, 4–8 h, (h) HOBt, EDC·HCl, DIPEA, DMF, rt. 4 h.

observing a 1 : 3 chloro pattern in mass spectrum. Compound **ANI-1** is subjected to an acid amine coupling with 5-nitrofuran-2-carboxylic acid (**6**) in the presence of HOBt, EDC·HCl, and DIPEA. This reaction resulted in the formation of 2-(4-(5-nitrofuran-2-carbonyl) piperazin-1-yl)-1,8-naphthyridine-3-carbonitrile (**ANA-12**). Confirmation of compound **ANA-12**, is done by observing amide carbonyl stretching frequency at 1694 cm^{-1} and nitro group frequency at 1370 cm^{-1} and 1570 cm^{-1} in IR spectrum. Subsequently, compound **ANI-2** is subjected to reaction with substituted anilines in the presence of Na_2CO_3 and KI in DMF. This reaction yielded the target compounds 2-(4-(phenylglycyl) piperazin-1-yl)-1,8-naphthyridine-3-carbonitrile (**ANC 1–14**). Likewise, compound **ANI-1** when subjected to reaction with substituted *N*-

Table 1 Anti-TB activity of the 1,8-naphthyridine derivatives against Mtb H37Rv strain

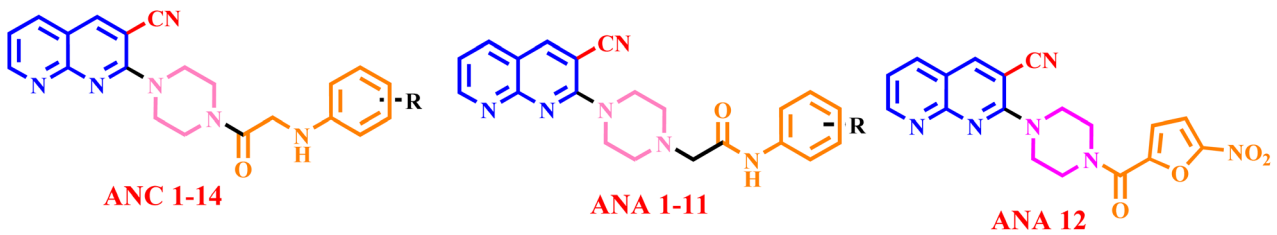

Entry	R	MIC[a] (μg mL^{-1}) (μM)
ANI-1	—	25 (104.480)
ANI-2	—	25 (79.17)
ANC-1	–H	25 (67.12)
ANC-2	–4-CH_2CH_3	12.5 (31.21)
ANC-3	–3,4-CH_3	50 (124.84)
ANC-4	–3,5-CH_3	>50 (>124.84)
ANC-5	–4-F	25 (67.12)
ANC-6	–4-Cl	25 (61.44)
ANC-7	–4-Br	25 (55.39)
ANC-8	–2-F	25 (64.03)
ANC-9	–2-I	25 (50.16)
ANC-10	–4-Br, 2-NO_2	>50 (>100.53)
ANC-11	–3-Cl	50 (122.88)
ANC-12	–3-CF_3	25 (56.76)
ANC-13	–2,4-Cl	50 (113.29)
ANC-14	–3,4-F	>50 (>122.42)
ANA-1	–H	12.5 (33.56)
ANA-2	–4-CH_2CH_3	25 (62.42)
ANA-3	–3,4-CH_3	25 (62.42)
ANA-4	–4-F	25 (64.03)
ANA-5	–4-Br	25 (55.39)
ANA-6	–2-F	12.5 (32.01)
ANA-7	–2-NO_2	12.5 (29.94)
ANA-8	–3-CF_3	12.5 (28.38)
ANA-9	–3,4-F	25 (61.21)
ANA-10	–3-NO_2	12.5 (29.94)
ANA-11	–4-NO_2	25 (59.80)
ANA-12	—	6.25 (16.52)
p-Amino salicylic acid	—	12.5 (81.62)
Ethambutol	—	6.25 (30.59)
Rifampicin	—	3.13 (3.79)
Isoniazid	—	0.36 (2.62)

[a] The assay was carried out in triplicates.

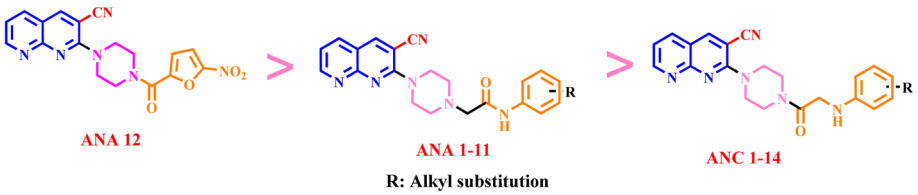

Fig. 5 Summary of the SAR of the ANC and ANA series compounds.

phenylacetamides in the presence of Na_2CO_3 and KI in DMF resulted in the target compounds 2-(4-(3-cyano-1,8-naphthyridin-2-yl) piperazin-1-yl)-*N*-phenylacetamide (**ANA 1–11**). The detailed spectral characterization of **ANC 1–14** and **ANA 1–11** is outlined in experimental section.

TLC and ESI mass spectrometry were utilized to monitor the progress of each reaction. For purification of the crude products at each stage, column chromatography employing silica gel (100 to 200 mesh size) and a gradient elution of EtOAc in hexane (ranging from 20% to 80%) were employed. Confirmation of the structures was achieved through the use of ^{1}H NMR, ^{13}C NMR, and ESI-MS. Detailed procedures for the synthesis of intermediates and final compounds are provided in the ESI.† The experimental section includes the physicochemical characteristics of the final compounds as well as analytical data.

Biological evaluation

***In vitro* anti-mycobacterial activity.** The study investigated the *in vitro* anti-mycobacterial activity of the titled compounds against the Mtb H37Rv strain using the Microplate Alamar Blue Assay (MABA) technique.[40] The evaluated compounds, including **ANI 1–2**, **ANC 1–14**, and **ANA 1–12**, displayed MIC against Mtb in the range of 6.25 to ≥50 μg mL^{-1}. Among all the synthesized derivatives, **ANA-12** exhibited the most potent anti-mycobacterial activity, with an MIC of 6.25 μg mL^{-1}. These results were compared to standard drugs such as rifampicin (MIC 3.13 μg mL^{-1}), ethambutol (MIC 6.25 μg mL^{-1}), and *p*-aminosalicylic acid (MIC 12.5 μg mL^{-1}). The anti-tubercular activity findings are summarized in Table 1.

Structure–activity relationship (SAR) studies. The anti-TB results, as the minimum inhibitory concentration (MIC) values, of the newly synthesized derivatives (**ANC 1–14**, and **ANA 1–12**) against Mtb H37Rv strain are shown in Table 1. Among the synthesized **ANA** derivatives, compound containing 5-nitrofuran heteroaromatic ring on piperazine, that is 2-(4-(5-nitrofuran-2-carbonyl) piperazin-1-yl)-1,8-naphthyridine-3-carbonitrile (**ANA-12**), exerted remarkable anti-tubercular activity with MIC value 6.25 μg mL^{-1} same as standard drug ethambutol (MIC 6.25 μg mL^{-1}). Among substituted *N*-phenyl-acetamide derivatives (**ANA 1–11**), compounds containing electron withdrawing group such as (–NO_2, –CF_3) exhibited good anti-TB activity (**ANA 7–8**, **ANA 10**) with an MIC value 12.5 μg mL^{-1}. Compounds with electron-donating alkyl substitutions, like (−3,4-CH_3), exhibit lower anti-TB activity (**ANA-3**) with a minimum inhibitory concentration (MIC) of 25 μg mL^{-1}. Other active compound from **ANA** series, **ANA-6**, with a halogen atom (–F), showed good anti-TB activity with an MIC value 12.5 μg mL^{-1}. Substituted aniline derivatives, particularly those with ethyl (–CH_2CH_3) substitution on the phenyl ring (**ANC-4**), demonstrated notable activity against tuberculosis, with MIC value of 12.5 μg mL^{-1}. Other compounds featuring alkyl substitutions and electron withdrawing groups on the phenyl ring displayed varying degrees of effectiveness against tuberculosis, ranging from moderate to weak activity. Fig. 5 illustrates a summary of the structure–activity relationship (SAR) studies.

Cytotoxicity studies. The compounds indicating the highest potency, with MIC values ≤ 12.5 μg mL^{-1}, underwent assessment for toxicity on the normal human embryonic kidney cell line (HEK293T). Following this, the most promising compounds were further investigated for their cytotoxic effects on HEK293T cells across a range of doses spanning from 7 to 2000 μM. The resulting IC_{50} values varied between 330 and 752.86 μM. The cell proliferation was measured at an OD of 450 nm. The investigation of selectivity index values revealed that the most potent compound, **ANA-12**, with a MIC of 6.25 μg mL^{-1}, exhibited strong selectivity, characterized by an SI > 27 (Table 2).[25,26]

***In silico* predicted ADME studies.** The physicochemical properties outlined in Lipinski's rule of five are essential for a new chemical molecule to be orally absorbed. Through *in silico* methods, these parameters can be predicted, aiding in the discovery of potential candidate molecules. Table S1† presents the *in silico* findings for the twenty-eight final analogues. The properties of the analogs, as predicted by the Lipinski rule, fell within the designated range for all parameters, such as molecular weight, hydrogen bond acceptor, hydrogen bond donor, and rule violations, except for the partition coefficient. All of the synthesized compounds follow with Lipinski's rule of five. Based on these anticipated outcomes, the final analogues seem not to pose pharmacokinetic concerns during drug development. The Swiss ADME tool was employed to forecast the characteristics of synthetic derivatives.[41] Based on the data the compounds demonstrate characteristics typical of drugs and show promising potential for effective oral absorption (Table S1†).

Molecular docking studies. Enoyl-ACP reductase (InhA) is an essential enzyme in fatty acid synthesis, particularly in the biosynthesis of mycolic acid. Belonging to the tyrosine-dependent oxidoreductase family, specifically the short dehydrogenase/reductase family, it's also recognized as an NADH-dependent enoyl-ACP reductase. InhA stands out as a promising target for the development of anti-TB drugs for several reasons. One key factor is its possession of a conserved

Table 2 Results of cytotoxicity studies on HEK293T cell line

S. No	Entry	MIC (μg mL^{-1}) (μM)	IC_{50}[a] (HEK293T) μM	Selective index (SI)
1	**ANC-2**	12.5 (31.21)	330 ± 3.40	11
2	**ANA-1**	12.5 (33.56)	580 ± 20.25	17
3	**ANA-6**	12.5 (32.01)	752.86 ± 7.63	23
4	**ANA-7**	12.5 (29.94)	571.19 ± 4.45	19
5	**ANA-12**	6.25 (16.52)	450.7 ± 20.21	27

[a] IC_{50} value is shown as mean ± SD. The assay was carried out in triplicates.

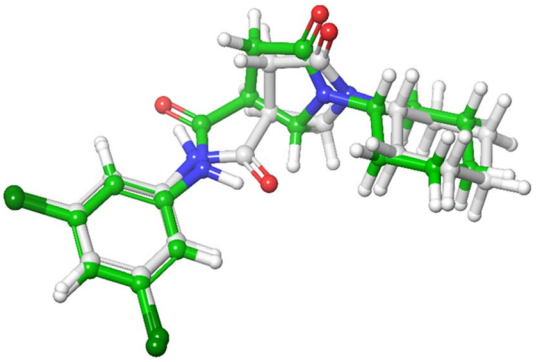

Fig. 6 Overlap position of re-docked pose of co-crystal ligand (white) with its X-ray pose (green) in the active site of the target (PDB-4TZK).

active site, a characteristic absent in many other targets within *Mycobacterium tuberculosis* (Mtb). Additionally, the active site of InhA features deep binding pockets, offering ample opportunities for the design and development of a diverse range of small molecule inhibitors to effectively bind and disrupt its function. InhA serves as the primary target for the anti-tubercular drug isoniazid and lacks a human ortholog. Consequently, directing efforts towards InhA continues to be the preferred strategy for developing drug molecules against *Mycobacterium tuberculosis*.[42,43]

Over the past twenty years, researchers worldwide have discovered numerous potent inhibitors of enoyl-ACP reductase (InhA). Most recently, our team also contributed to this effort by identifying new InhA inhibitors with potential anti-TB activity.[44,45] Literature reports indicate that the presumed mechanism of action of anti-mycobacterial naphthyridine compounds involves inhibiting InhA.[46] Hence, we selected the InhA enzyme, with PDB ID 4TZK, as the target for conducting docking studies of our compounds, which are based on the naphthyridine nucleus. We conducted molecular docking studies of the most active anti-TB compound **ANA-12** against Mtb InhA (PDB ID 4TZK). This allowed us to predict how the ligands would bind within the active site of the target enzyme InhA. The crystal structure of InhA (PDB ID 4TZK) was obtained from the Protein Data Bank with a resolution of 1.62 Å. Initially, the docking protocol underwent validation by removing the ligand from the crystal structure and then re-docking it into the same binding site to assess the precision and trustworthiness of the docking method. An RMSD of 0.4 Å for the target protein signifies a reasonably precise prediction of the binding pose, indicating that the docking protocol is capable of replicating the native ligand conformation with commendable accuracy (Fig. 6).

The binding interactions of co-crystallized ligand and most active compound **ANA-12** at the binding site were tabulated in Table 3. The docking score of co-crystal ligand is −11.08 kcal mol^{-1}, while that of the most active compound **ANA-12** was −8.424 kcal mol^{-1}, respectively. The docked orientation of the co-crystallized ligand revealed that the amino acid residue TYR-158, (distance 1.99 Å), is engaged in a hydrogen bond with the protein. Furthermore, aromatic bonding interactions with PRO-156 (distance 2.57 Å) and halogen bonding interactions with GLY-104 (distance 3.02 Å) were observed alongside the hydrogen bonding (Fig. 7). These various interactions collectively enhanced the stability of the co-crystallized ligand within the active site of the target protein, consequently contributing to a notable increase in the docking score. It was observed that, the amino-acid LYS-165 was found to be involved in the salt bridge interaction with the compound **ANA-12** (distance 4.53 Å). Furthermore, same amino-acid LYS-165 (distance 1.89 Å). was found to be involved in the hydrogen bond interaction with nitro oxygen of the compound

Table 3 Summary of key residues involved in the interactions with co-crystal ligand and compound **ANA-12** along with docking score against target protein 4TZK

	Amino acid involved in the interactions	Type of bond	Distance (Å)	Glide score (kcal mol^{-1})
Co-crystal ligand	TYR-158	Hydrogen bond	1.99	−11.08
	PRO-156	Aromatic bond	2.57	
	GLY-104	Halogen bond	3.02	
ANA-12	LYS-165	Salt bridge	4.53	−8.424
	LYS-165	Hydrogen bond	1.89	

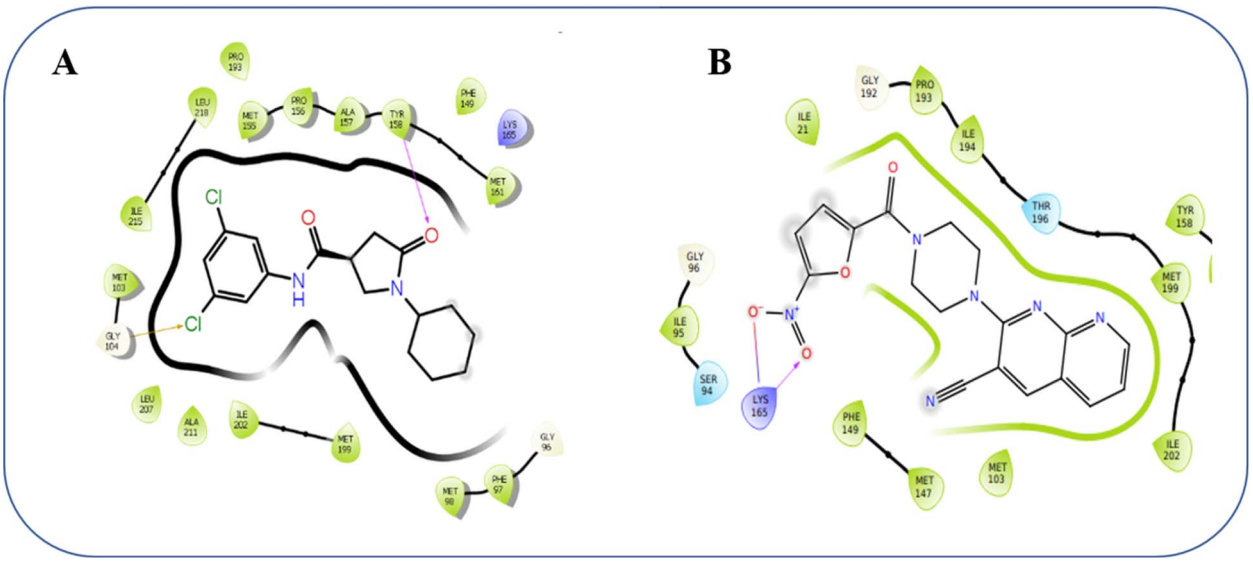

Fig. 7 2D interaction map of the reference co-crystal ligand (A) and active compound **ANA-12** (B) docked against target protein InhA (PDB: 4TZK).

ANA-12 (Fig. 7). Due to these strong binding patterns, compound **ANA-12** exhibited considerable potency against mycobacterial activity, demonstrating a MIC 6.25 μg mL^{-1}.

Molecular dynamic (MD) simulation analysis. MD simulations were conducted to investigate the stability, conformation, and intermolecular interactions of the ligand molecules bound to the InhA target. The academic version of the Desmond module (Version 2020-4) was employed to compute the time-dependent dynamic alterations of docked complexes. Simulations utilizing the TIP3P water model were conducted at

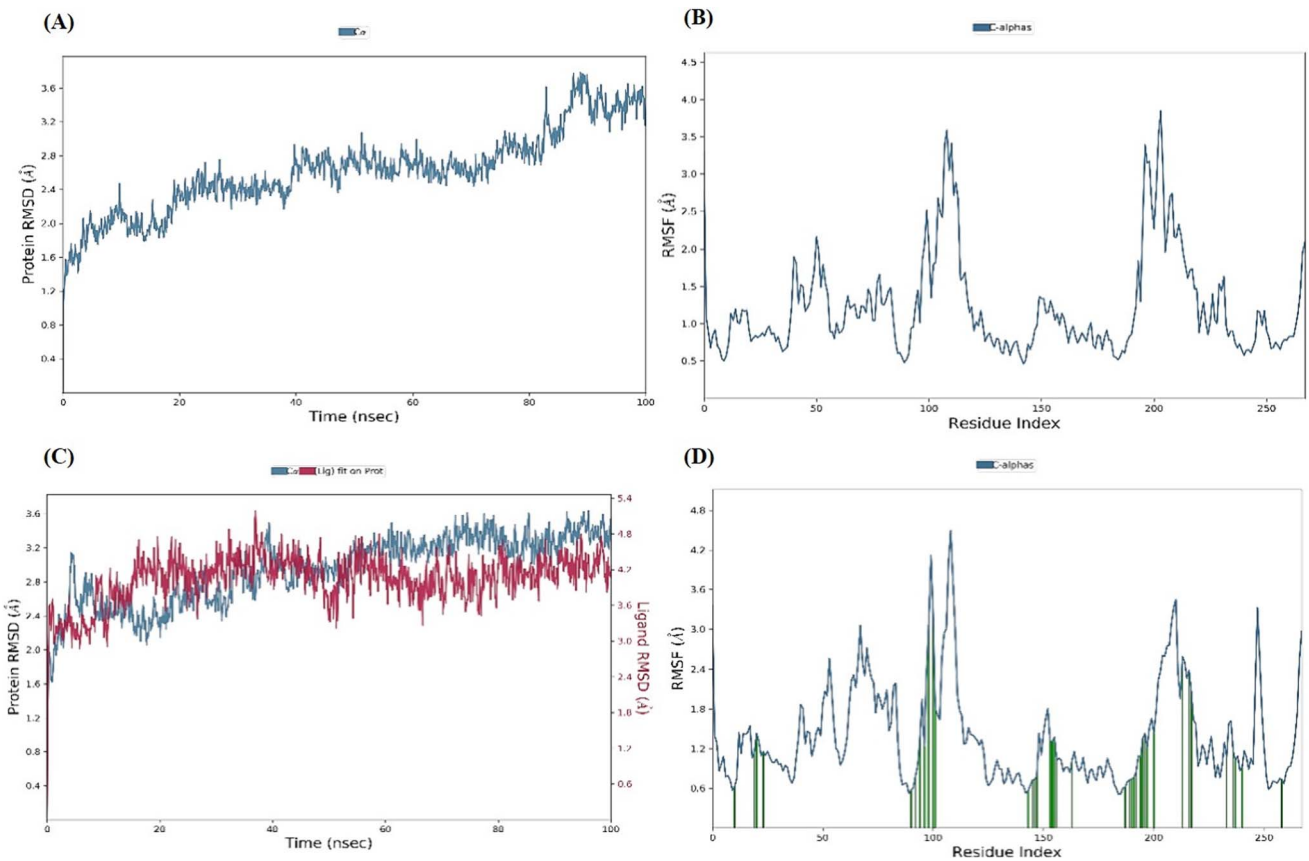

Fig. 8 RMSD and RMSF plots of apoprotein (A and B) and most active compound **ANA-12** (C and D) during the MD simulation.

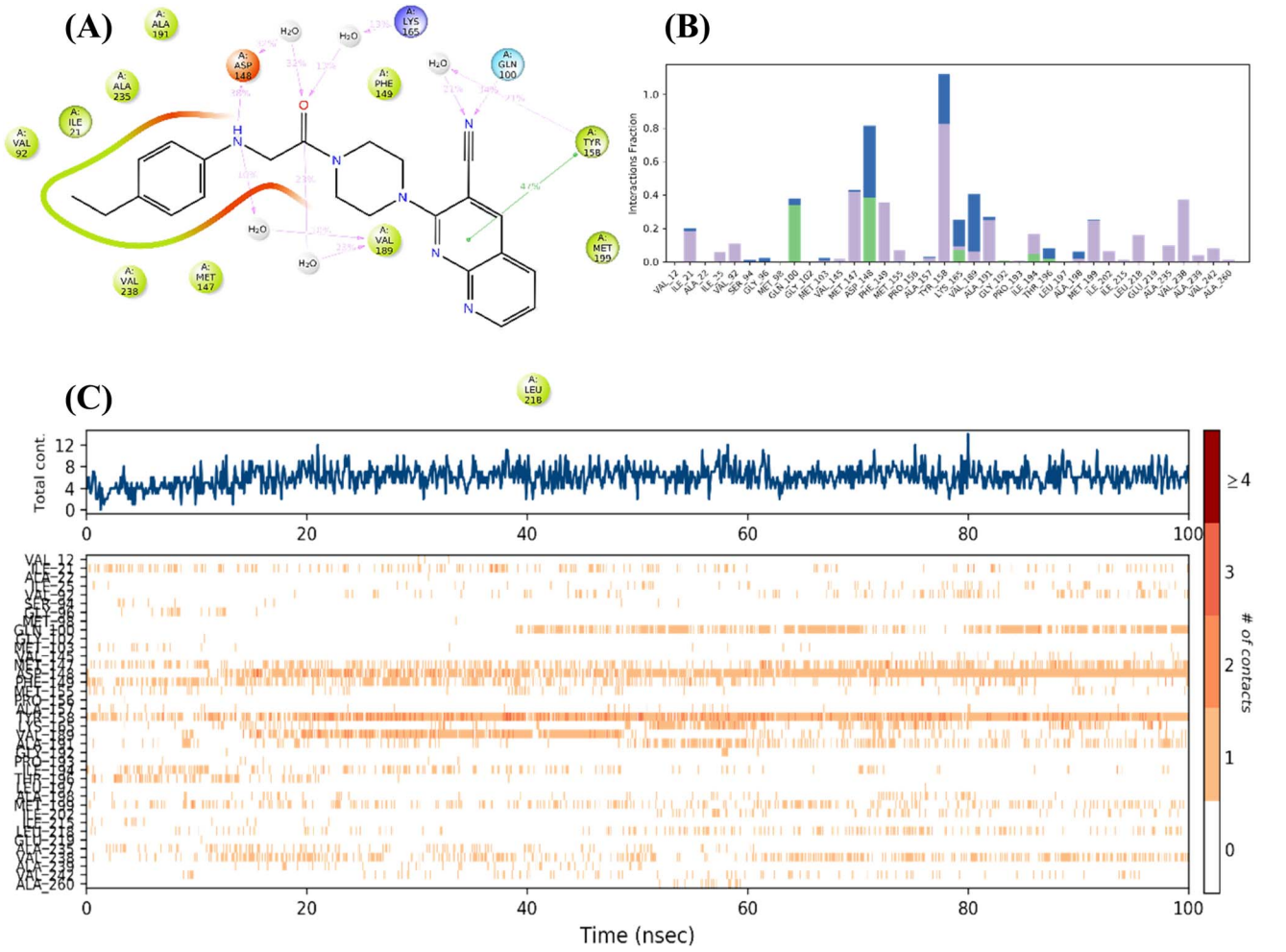

Fig. 9 4TZK protein and compound **ANA-12** interactions during the MD simulation. (A) Percentage of amino acid interactions (B) vital amino acid interactions (C) binding pattern of the compound **ANA-12** within the active site.

a temperature of 310.15 K and pressure of 1.01 bar, while employing the OPLS4 force field for a duration of 100 ns.

This study investigated the flexibility and stability of the complex **ANA-12** compared to the apoenzyme. The protein root mean square deviation (RMSD) of the apoenzyme remained below 3.6 Å, showing a linear increase in RMSD values up to 89 ns before reaching stability (Fig. 8A). Conversely, **ANA-12** displayed an initial drift in RMSD values, reaching up to 3.2 Å within the first 5 ns. Subsequently, RMSD values fluctuated below 3 Å up to 40 ns without achieving stability, possibly due to inadequate coordination with specific residues like MET147, ASP148, PHE149, and VAL189. Following this phase, the protein stabilized with values consistently below 3.5 Å for the remainder of the simulation, demonstrating strong coordination with GLN100, ASP148, and TYR158 (Fig. 8C). Moreover, the root mean square fluctuation (RMSF) plot revealed the flexibility and dynamic behavior of residues within the protein. In the **ANA-12** complex, higher RMSF values (below 4.2 Å) were noted between residues 90 to 100, indicating increased flexibility in those regions upon ligand binding. However, other ligand contact regions exhibited lower RMSF values below 2 Å, suggesting minimal fluctuation at the binding site of the target 4TZK protein (Fig. 8B and D).

Fig. 9 illustrates the binding pattern of the compound **ANA-12** within the active site of the 4TZK protein. The protein-ligand interactions observed in molecular docking studies were consistent in the MD results. The **ANA-12** complex predominantly engaged in hydrophobic interactions, followed by water-mediated and hydrogen bond interactions. Notably, the complex was significantly stabilized by hydrophobic interactions with TYR158, which accounted for approximately 47% of the simulation time. Residues such as MET147, PHE149, ALA191, MET199, LEU218, and VAL238 also contributed to the complex stabilization through hydrophobic interactions. During the simulation, specific residues, including ASP148 (about 32%), TYR158 (about 21%), LYS165 (about 13%), and VAL189 (about 33%), actively participated in water-mediated hydrogen bonding with the amine, carbonyl, and cyano groups of **ANA-12**. Furthermore, hydrogen bond interactions with GLN100 and ASP148, contributing approximately 34% and 38% of the simulation time respectively, further strengthened

Table 4 Crystal data and structure refinement for compound ANC-5

Identification code	ANC-5
Hall group	$P\bar{1}$
Moiety formula	$C_{21}H_{19}FN_6O$
Sum formula	$C_{21}H_{19}FN_6O$
Molecular weight	390.42
Dx, g cm^{-3}	1.46
Z	2
Temperature (K)	126
Mu (mm^{-1})	0.842
F000	408
F000′	409.28
h, k, l_{max}	7, 9, 26
N_{ref}	3744
T_{min}, T_{max}	0.746, 1.000

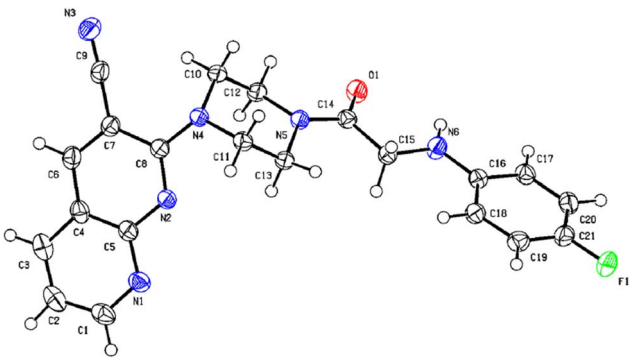

Fig. 10 ORTEP diagram of crystal ANC-5.

the complex. Notably, the cyano group and secondary amine of **ANA-12** were involved in these interactions.

Single crystal X-ray crystallographic structure of compound ANC-5. To better understand the arrangement of **ANC-5** compound, crystals were grown for single-crystal X-ray diffraction (SCXRD) examination using a mixture comprising a 1 : 9 ratio of MeOH to DCM.

The SCXRD measurements were performed on the Rigaku XtaLAB P200 diffractometer using graphite monochromated Cu Kα radiation (λ = 1.54184 Å). The CrysAlisPro software by Rigaku Oxford Diffraction was utilized for data acquisition and reduction. Data gathering occurred at a temperature of 126 K. Structure resolution was achieved through Olex2, employing the ShelX program's direct methods, and refinement was executed using the ShelXL package's least squares minimization. The fundamental crystallographic data is presented in the accompanying Table 4.

The molecular structure of the compound **ANC-5** of ORTEP diagram (Fig. 10) contains one linker per asymmetric unit (Fig. 11) with the chemical formula ($C_{21}H_{19}FN_6O$), and the structure crystallizes in the triclinic crystal system. From the crystallographic data for the compound **ANC-5** has been deposited to the Cambridge Crystallographic Data Center, and the corresponding deposition number is CCDC 2342616.

Conclusion

In conclusion, we have designed and synthesized, twenty-eight derivatives of 1,8-naphthyridine-3-carbonitriles (**ANC** and **ANA**), which were subsequently tested for their *in vitro* anti-tubercular activity against the Mtb H37Rv strain. The synthesized derivatives were confirmed through ^{1}HNMR, ^{13}CNMR, LC-MS, and elemental analyses. These compounds demonstrated significant to moderate anti-tubercular activity. Notably, **ANA-12** exhibited outstanding anti-TB efficacy with a MIC of 6.25 μg mL^{-1}, as determined by the MABA method. Structure activity relationship studies indicate that among all the synthesized 1,8-naphthyridine derivatives, compound containing 5-nitrofuran heteroaromatic ring on piperazine, *i.e.*, **ANA-12** exerted remarkable anti-tubercular activity with MIC 6.25 μg mL^{-1} as compared to substituted anilines (**ANC 1–14**) and *N*-phenylacetamide (**ANA 1–11**) derivatives. It was observed that all these compounds were nontoxic to normal human cells against HEK cells (human embryonic kidney cells). In a molecular docking study, the co-crystal ligand achieved a docking score of −11.08 kcal mol^{-1}, whereas the most active compound, **ANA-12**, had a docking score of −8.424 kcal mol^{-1}. The molecular dynamics study investigated the flexibility and stability of the complex **ANA-12** compared to the apoenzyme. The protein root

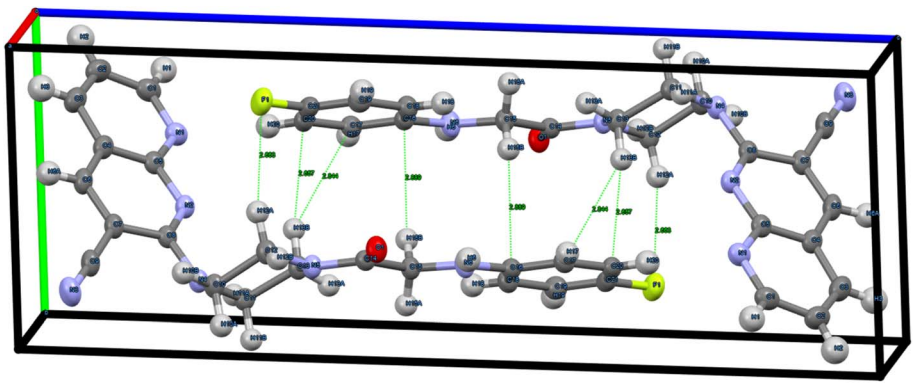

Fig. 11 Packing diagrams of compound ACN-5 along the *b* axes. C, H, N, O and F atoms are shown in grey, white, blue, red and yellow colours, respectively.

mean square deviation (RMSD) of the apoenzyme remained below 3.6 Å, showing a linear increase in RMSD values up to 89 ns before reaching stability. Additionally, the *in silico* ADMET values predicted for these compounds fell within the range observed for marketed drugs. A single-crystal structure was also established for compound **ANA-5**, providing additional confirmation of the structures of its analogs. In the future, the most active compounds, such as **ANA-12**, with anti-TB activity, can be subjected to *in vivo* studies to understand their effects in living organisms. Based on the docking results of the most active compound, further molecules can be developed that may exhibit even more potent activity than the current findings.

Experimental section

Chemistry

General procedure for preparation of intermediates and final compounds. The general procedure for preparing intermediates and final compounds is detailed in the ESI† section.

Analytical data for the final compounds (ANI 1–2, ANC 1–14, ANA 1–12)

*2-(Piperazin-1-yl)-1,8-naphthyridine-3-carbonitrile (**ANI-1**).* Yellow solid; yield (75%), m.p. 221–223 °C. IR (KBr, υ_{max}/cm^{-1}): 3368, 2853, 2242, 1594, 1499. ^{1}H NMR (400 MHz, DMSO-d_6) δ 8.96 (dd, J = 4.4, Hz, 1H), 8.93 (s, 1H), 8.29 (dd, J = 8.0, Hz, 1H), 7.43 (dd, J = 8.0, Hz, 1H), 3.67–3.63 (m, 4H), 2.89–2.85 (m, 4H), 1.23 (s, 1H). ^{13}C NMR (101 MHz, DMSO-d_6) δ 161.78, 159.88, 158.29, 156.40, 148.88, 146.36, 137.84, 120.86, 118.40, 116.84, 98.87, 50.46, 45.48. ESI MS (m/z): calcd. For $C_{13}H_{13}N_5$, 239.28, found 240.15 [M + H]$^+$. Anal. calcd for $C_{13}H_{13}N_5$ (%) C, 65.25; H, 5.48; N, 29.27 found: C, 65.20; H, 5.50; N, 29.23.

*2-(4-(2-Chloroacetyl) piperazin-1-yl)-1,8-naphthyridine-3-carbonitrile (**ANI-2**).* Dark brown solid; yield (73%), m.p. 258–260 °C. IR (KBr, υ_{max}/cm^{-1}): 3051, 2242, 1659, 1602, 1458. ^{1}H NMR (400 MHz, DMSO-d_6) δ 8.99 (m, J = 2.1 Hz, 1H), 8.33 (dd, J = 8.0, 2.0 Hz, 1H), 7.47 (dd, J = 8.0, 4.4 Hz, 1H), 4.48 (s, 2H), 3.85–3.74 (m, 4H), 3.70–3.67 (m, Hz, 4H). ^{13}C NMR (101 MHz, DMSO-d_6) δ 165.55, 159.23, 156.76, 155.73, 153.92, 149.24, 138.48, 121.22, 118.38, 117.41, 98.91, 49.18, 48.27, 42.56. ESI MS (m/z): calcd. For $C_{15}H_{14}ClN_5O$, 315.76, found 338.10 [M + Na]$^+$. Anal. calcd for $C_{15}H_{14}ClN_5O$ (%) C, 57.06; H, 4.47; Cl, 11.23; N, 22.18; O, 5.07 found: C, 57.01; H, 4.53; Cl, 11.20; N, 22.23; O, 5.09.

*2-(4-(Phenylglycyl) piperazin-1-yl)-1,8-naphthyridine-3-carbonitrile (**ANC-1**).* Brown solid; yield (72%), m.p. 161–163 °C. IR (KBr, υ_{max}/cm^{-1}): 3354, 2916, 2242, 2223, 1690,1493. ^{1}H NMR (400 MHz, DMSO-d_6) δ 8.99 (d, J = 2.8 Hz, 2H), 8.36–8.30 (m, 1H), 7.47 (dd, J = 8.0, Hz, 1H), 7.09 (dd, J = 8.4, Hz, 2H), 6.71–6.66 (m, 2H), 6.57 (t, J = 7.3 Hz, 1H), 5.59 (s, 1H), 3.99 (s, 2H), 3.86–3.77 (m, 4H), 3.75–3.73 (m, 4H). ^{13}C NMR (101 MHz, DMSO-d_6) δ 167.90, 161.40, 155.22, 153.45, 147.84, 135.91, 129.12, 129.12, 122.28, 118.81, 118.27, 116.25, 114.31, 114.25, 99.32, 48.00, 48.00, 44.84, 44.51. ESI MS (m/z): calcd. For $C_{21}H_{20}N_6O$, 372.43, found 373.25 [M + H]$^+$. Anal. calcd for $C_{21}H_{20}N_6O$ (%) C, 67.73; H, 5.41; N, 22.57; O, 4.30 found: C, 67.63; H, 5.30; N, 22.60; O, 4.27.

*2-(4-((4-Ethylphenyl)glycyl)piperazin-1-yl)-1,8-naphthyridine-3-carbonitrile (**ANC-2**).* Brown solid; yield (69%), m.p. 158–159 °C. IR (KBr, υ_{max}/cm^{-1}): 3350, 3016, 2244, 2221, 1680,1491. ^{1}H NMR (400 MHz, DMSO-d_6) δ 9.01–8.97 (m, 2H), 8.36–8.31 (m, 1H), 7.51–7.44 (m, 2H), 7.13 (d, J = 2.3 Hz, 1H), 6.93 (d, J = 8.5 Hz, 2H), 6.67 (d, J = 8.3 Hz, 1H), 6.61 (d, J = 8.5 Hz, 2H), 3.96 (s, 2H), 3.80–3.78 (m, 4H), 3.74–3.70 (m, 4H), 2.48–2.42 (q, 2H), 1.11 (t, J = 7.6 Hz, 3H). ^{13}C NMR (101 MHz, DMSO-d_6) δ 166.83, 164.85, 159.89, 157.31, 149.46, 146.06, 141.60, 137.87, 131.90, 128.72, 119.65, 117.74, 112.04, 107.38, 48.25, 31.92, 29.32, 16.83. ESI MS (m/z): calcd. For $C_{23}H_{24}N_6O$, 400.49, found 423.25 [M + Na]$^+$. Anal. calcd for $C_{23}H_{24}N_6O$ (%) C, 68.98; H, 6.04; N, 20.99; O, 3.99 found: C, 68.90; H, 6.15; N, 20.01; O, 3.97.

*2-(4-((3,4-Dimethylphenyl)glycyl)piperazin-1-yl)-1,8-naphthyridine-3-carbonitrile (**ANC-3**).* Brown solid; yield (66%), m.p. 148–150 °C. IR (KBr, υ_{max}/cm^{-1}): 3349, 2243, 2021, 1677,1483. ^{1}H NMR (400 MHz, DMSO-d_6) δ 9.01–8.97 (m, 2H), 8.35–8.29 (m, 1H), 7.47 (dd, J = 8.0, Hz, 1H), 6.84 (d, J = 8.1 Hz, 1H), 6.51 (d, J = 1.6 Hz, 1H), 6.42 (dd, J = 8.0, Hz, 1H), 5.25 (s, 1H), 3.94 (s, 2H), 3.85–3.80 (m, 4H), 3.74–3.71 (m, 4H), 2.12 (s, 3H), 2.07 (s, 3H). ^{13}C NMR (101 MHz, DMSO-d_6) δ 169.31, 158.58, 157.05, 155.84, 149.51, 146.96, 137.83, 136.64, 130.27, 124.00, 121.21, 117.65, 114.67, 110.54, 99.16, 48.50, 48.08, 45.53, 20.20, 18.85. ESI MS (m/z): calcd. For $C_{23}H_{24}N_6O$, 400.49, found 399.10 [M–H]$^-$. Anal. calcd for $C_{23}H_{24}N_6O$ (%) C, 68.98; H, 6.04; N, 20.99; O, 3.99 found: C, 68.93; H, 6.12; N, 20.04; O, 3.92.

*2-(4-((3,5-Dimethylphenyl)glycyl)piperazin-1-yl)-1,8-naphthyridine-3-carbonitrile (**ANC-4**).* Dark brown solid; yield (58%), m.p. 151–152 °C. IR (KBr, υ_{max}/cm^{-1}): 3347, 3010, 2217, 1670, 1456. ^{1}H NMR (400 MHz, DMSO-d_6) δ 9.01–8.96 (m, 2H), 8.34–8.30 (m, 1H), 7.47 (dd, J = 8.0, Hz, 1H), 6.30 (s, 2H), 6.22 (s, 1H), 5.35 (s, 1H), 3.96 (s, 2H), 3.85–3.77 (m, 4H), 3.74–3.72 (m, 4H), 2.15 (s, 6H). ^{13}C NMR (101 MHz, DMSO-d_6) δ 168.67, 159.03, 156.75, 155.50, 149.81, 148.28, 137.87, 121.85, 120.87, 118.69, 111.41, 99.20, 48.50, 45.42, 21.51. ESI MS (m/z): calcd. For $C_{23}H_{24}N_6O$, 400.49, found 423.20 [M + Na]$^+$. Anal. calcd for $C_{23}H_{24}N_6O$ (%) C, 68.98; H, 6.04; N, 20.99; O, 3.99 found: C, 68.89; H, 6.10; N, 20.10; O, 3.90.

*2-(4-((4-Fluorophenyl)glycyl)piperazin-1-yl)-1,8-naphthyridine-3-carbonitrile (**ANC-5**).* Brown solid; yield (74%), m.p. 129–130 °C. IR (KBr, υ_{max}/cm^{-1}): 3353, 3012, 2228, 1670, 1446. ^{1}H NMR (400 MHz, DMSO-d_6) δ 9.01–8.96 (m, 2H), 8.36–8.29 (m, 1H), 7.47 (dd, J = 8.0, Hz, 1H), 6.96–6.88 (m, 2H), 6.70–6.64 (m, 3H), 5.58 (s, 1H), 3.97 (s, 2H), 3.87–3.78 (m, 4H), 3.74–3.70 (m, 4H). ^{13}C NMR (101 MHz, DMSO-d_6) δ 168.70, 158.94, 156.75, 155.49, 153.93, 153.57, 148.91, 145.40, 138.19, 120.85, 117.08, 115.79, 113.68, 98.93, 48.21, 45.42. ESI MS (m/z): calcd. For $C_{21}H_{19}FN_6O$, 372.43, found 389.05 [M–Na]$^-$. Anal. calcd for $C_{21}H_{19}FN_6O$ (%) C, 64.60; H, 4.91; F, 4.87; N, 21.53; O, 4.10 found: C, 64.58; H, 4.93; F, 4.80; N, 21.64; O, 4.09.

*2-(4-((4-Chlorophenyl)glycyl)piperazin-1-yl)-1,8-naphthyridine-3-carbonitrile (**ANC-6**).* Brown solid; yield (72%), m.p. 171–172 °C. IR (KBr, υ_{max}/cm^{-1}): 3350, 3015, 2219, 1670, 1483. ^{1}H NMR (400 MHz, DMSO-d_6) δ 8.99 (s, 2H), 8.32 (dd, J = 7.9, Hz, 1H), 7.47 (dd, J = 8.0, 4.3 Hz, 2H), 7.10 (d, J = 8.8 Hz, 1H), 6.70 (d, J =

8.8 Hz, 2H), 5.86 (s, 1H), 4.00 (s, 2H), 3.80–3.78 (m, 4H), 3.74–3.72 (m, 4H). ^{13}C NMR (101 MHz, DMSO-d_6) δ 168.67, 162.43, 159.23, 157.03, 155.78, 147.63, 138.24, 129.39, 120.85, 119.31, 118.02, 116.16, 114.36, 111.80, 98.94, 47.90, 45.07. ESI MS (m/z): calcd. For $C_{21}H_{19}ClN_6O$, 406.87, found 407.20 $[M + H]^+$. Anal. calcd for $C_{21}H_{19}ClN_6O$ (%) C, 61.99; H, 4.71; Cl, 8.71; N, 20.66; O, 3.93 found: C, 61.90; H, 4.75; Cl, 8.77; N, 20.60; O, 3.96.

*2-(4-((4-Bromophenyl)glycyl)piperazin-1-yl)-1,8-naphthyridine-3-carbonitrile (**ANC-7**).* Brown solid; yield (65%), m.p. 160–162 °C. IR (KBr, υ_{max}/cm^{-1}): 3354, 2244, 2220, 1682,1483. ^{1}H NMR (400 MHz, DMSO-d_6) δ 8.99 (d, J = 3.1 Hz, 2H), 8.36–8.28 (m, 1H), 7.47 (dd, J = 8.0, Hz, 1H), 7.23–7.19 (m, 2H), 6.69–6.63 (m, 2H), 5.89 (s, 1H), 3.99 (s, 2H), 3.86–3.77 (m, 4H), 3.75–3.64 (m, 4H). ^{13}C NMR (101 MHz, DMSO-d_6) δ 168.66, 159.24, 156.74, 156.10, 149.83, 147.89, 147.61, 138.47, 132.16, 121.47, 118.36, 118.00, 116.84, 114.94, 107.03, 98.53, 47.93, 45.11. ESI MS (m/z): calcd. For $C_{21}H_{19}BrN_6O$, 451.33, found 453.15 $[M + H]^+$. Anal. calcd for $C_{21}H_{19}BrN_6O$ (%) C, 55.89; H, 4.24; Br, 17.70; N, 18.62; O, 3.54 found: C, 55.85; H, 4.20; Br, 17.73; N, 18.62; O, 3.50.

*2-(4-((2-Fluorophenyl)glycyl)piperazin-1-yl)-1,8-naphthyridine-3-carbonitrile (**ANC-8**).* Brown solid; yield (66%), m.p. 144–145 °C. IR (KBr, υ_{max}/cm^{-1}): 3351, 3014, 2217, 1670, 1484. ^{1}H NMR (400 MHz, DMSO-d_6) δ 8.85 (s, 1H), 8.65 (s, 1H), 8.26 (s, 1H), 7.47 (s, 1H), 6.93 (d, J = 6.7 Hz, 2H), 6.79 (s, 1H), 6.65 (s, 1H), 4.11 (s, 1H), 3.88–3.77 (m, 4H), 3.70–3.66 (m, 2H), 3.47–3.43 (m, 2H). ^{13}C NMR (101 MHz, DMSO-d_6) δ 167.90, 161.40, 155.22, 153.45, 152.24, 135.91, 134.61, 125.62, 122.28, 118.81, 117.94, 117.59, 116.25, 114.31, 99.32, 48.00, 48.00, 44.84, 44.84, 44.47. ESI MS (m/z): calcd. For $C_{21}H_{19}FN_6O$, 390.42, found 413.20 $[M + Na]^+$. Anal. calcd for $C_{21}H_{19}FN_6O$ (%) C, 64.60; H, 4.91; F, 4.87; N, 21.53; O, 4.10 found: C, 64.51; H, 4.90; F, 4.85; N, 21.56; O, 4.13.

*2-(4-((2-Iodophenyl)glycyl)piperazin-1-yl)-1,8-naphthyridine-3-carbonitrile (**ANC-9**).* Dark Brown solid; yield (65%), m.p. 147–148 °C. IR (KBr, υ_{max}/cm^{-1}): 3349, 2926, 2247, 2219, 1685,1473. ^{1}H NMR (400 MHz, DMSO-d_6) δ 8.88 (s, 1H), 8.64 (s, 1H), 8.25 (s, 1H), 7.56 (s, 1H), 6.56 (d, J = 1.4 Hz, 1H), 6.51 (d, J = 14.4 Hz, 1H), 4.09 (s, 1H), 3.72–3.68 (m, 4H), 3.48–3.44 (m, 2H). ^{13}C NMR (101 MHz, DMSO-d_6) δ 167.90, 161.40, 155.22, 153.45, 144.53, 139.91, 135.91, 128.18, 122.28, 121.68, 114.31, 113.92, 99.90, 99.32, 48.00, 48.00, 44.84, 44.84, 44.47. ESI MS (m/z): calcd. For $C_{21}H_{19}IN_6O$, 498.33, found 499.15 $[M + H]^+$. Anal. calcd for $C_{21}H_{19}IN_6O$ (%) C, 50.62; H, 3.84; I, 25.47; N, 16.86; O, 3.21 found: C, 50.56; H, 3.79; I, 25.40; N, 16.91; O, 3.20.

*2-(4-((4-Bromo-2-nitrophenyl)glycyl)piperazin-1-yl)-1,8-naphthyridine-3-carbonitrile (**ANC-10**).* Dark red solid; yield (68%), m.p. 157–159 °C. IR (KBr, υ_{max}/cm^{-1}): 3352, 2921, 2245, 1673,1476. ^{1}H NMR (400 MHz, DMSO-d_6) δ 8.87 (s, 1H), 8.63 (s, 1H), 8.24 (d, J = 11.6 Hz, 2H), 7.65 (s, 1H), 7.47 (s, 1H), 6.78 (s, 1H), 6.28 (s, 1H), 4.42 (s, 1H), 4.07 (s, 2H), 3.79–3.75 (m, 2H), 3.71–3.67 (m, 2H), 3.50–3.46 (m, 2H), 3.34–3.30 (m, 2H). ^{13}C NMR (101 MHz, DMSO-d_6) δ 156.80, 150.45, 146.36, 143.52, 138.82, 137.23, 131.94, 130.99, 128.15, 122.51, 118.36, 105.78, 49.84, 44.17. ESI MS (m/z): calcd. For $C_{21}H_{18}BrN_7O_3$, 497.33, found 496.95 $[M–H]^-$. Anal. calcd for $C_{21}H_{18}BrN_7O_3$ (%) C, 50.82; H, 3.66; Br, 16.10; N, 19.75; O, 9.67 found: C, 50.75; H, 3.60; Br, 16.11; N, 19.70; O, 9.70.

*2-(4-((3-Chlorophenyl)glycyl)piperazin-1-yl)-1,8-naphthyridine-3-carbonitrile (**ANC-11**).* Brown solid; yield (74%), m.p. 152–154 °C. IR (KBr, υ_{max}/cm^{-1}): 3352, 2910, 2244, 2214, 1672,1463. ^{1}H NMR (400 MHz, DMSO-d_6) δ 8.99 (dd, J = 3.8, Hz, 1H), 8.33 (dd, J = 8.1, Hz, 1H), 7.95 (s, 1H), 7.48–7.44 (m, 1H), 7.07 (m, J = 8.0 Hz, 1H), 6.99 (d, J = 8.0 Hz, 1H), 6.78–6.71 (m, 1H), 5.98 (m, J = 5.0 Hz, 1H), 3.83 (s, 2H), 3.76–3.74 (m, 4H), 3.70–3.67 (m, 4H). ^{13}C NMR (101 MHz, DMSO-d_6) δ 168.38, 162.46, 158.95, 157.32, 156.14, 151.10, 149.48, 149.25, 145.07, 137.86, 134.06, 130.34, 121.49, 118.66, 113.64, 112.99, 112.42, 98.56, 48.89, 44.79. ESI MS (m/z): calcd. For $C_{21}H_{19}ClN_6O$, 406.87, found 405.00 $[M–H]^-$. Anal. calcd for $C_{21}H_{19}ClN_6O$ (%) C, 61.99; H, 4.71; Cl, 8.71; N, 20.66; O, 3.93 found: C, 61.90; H, 4.75; Cl, 8.77; N, 20.60; O, 3.90.

*2-(4-((3-(Trifluoromethyl)phenyl)glycyl)piperazin-1-yl)-1,8-naphthyridine-3-carbonitrile (**ANC-12**).* Brown solid; yield (59%), m.p. 153–154 °C. IR (KBr, υ_{max}/cm^{-1}): 3355, 3011, 2213, 1672, 1483. ^{1}H NMR (400 MHz, DMSO-d_6) δ 9.00–8.95 (m, 2H), 8.44 (s, 1H), 7.95 (s, 1H), 7.47 (dd, J = 8.0, Hz, 2H), 7.20 (t, J = 7.9 Hz, 1H), 7.02–6.90 (m, 2H), 4.07 (s, 2H), 3.82–3.80 (m, 4H), 3.83–3.64 (m, 4H). ^{13}C NMR (101 MHz, DMSO-d_6) δ 166.40, 164.89, 163.01, 158.95, 157.02, 150.48, 148.90, 142.87, 129.69, 128.42, 118.02, 36.63, 31.25. ESI MS (m/z): calcd. For $C_{22}H_{19}F_3N_6O$, 440.43, found 463.20 $[M + Na]^+$. Anal. calcd for $C_{22}H_{19}F_3N_6O$ (%) C, 60.00; H, 4.35; F, 12.94; N, 19.08; O, 3.63 found: C, 60.05; H, 4.30; F, 12.90; N, 19.11; O, 3.60.

*2-(4-((2,4-Dichlorophenyl)glycyl)piperazin-1-yl)-1,8-naphthyridine-3-carbonitrile (**ANC-13**).* Brown solid; yield (63%), m.p. 154–155 °C. IR (KBr, υ_{max}/cm^{-1}): 3354, 2223, 1670, 1480. ^{1}H NMR (400 MHz, DMSO-d_6) δ 9.00 (d, J = 2.6 Hz, 2H), 8.38–8.30 (m, 2H), 7.77–7.66 (m, 2H), 7.41 (d, J = 2.4 Hz, 1H), 7.06 (dd, J = 8.7 Hz, 1H), 6.78 (d, J = 8.7 Hz, 15H), 5.50 (s, 2H), 4.18–4.08 (m, 4H), 3.75 (m, 4H). ^{13}C NMR (101 MHz, DMSO-d_6) δ 167.90, 161.40, 155.22, 153.45, 141.83, 135.91, 130.90, 127.93, 123.93, 123.73, 122.28, 118.81, 116.25, 115.87, 99.32, 48.00, 44.84, 44.84, 44.47. ESI MS (m/z): calcd. For $C_{21}H_{18}Cl_2N_6O$, 441.32, found 463.10 $[M + Na]^+$. Anal. calcd for $C_{21}H_{18}Cl_2N_6O$ (%) C, 57.15; H, 4.11; Cl, 16.07; N, 19.04; O, 3.63 found: C, 57.10; H, 4.15; Cl, 16.09; N, 19.01; O, 3.56.

*2-(4-((3,4-Difluorophenyl)glycyl)piperazin-1-yl)-1,8-naphthyridine-3-carbonitrile (**ANC-14**).* Brown solid; yield (67%), m.p. 164–165 °C. IR (KBr, υ_{max}/cm^{-1}): 3352, 3013, 2225, 1680, 1483. ESI MS (m/z): calcd ^{1}H NMR (400 MHz, DMSO-d_6) δ 8.99 (dd, J = 4.5, Hz, 2H), 8.33 (dd, J = 8.1, 2H), 7.47 (dd, J = 8.0, Hz, 1H), 6.77–6.66 (m, 2H), 6.54–6.47 (m, 5H), 5.89 (m, J = 4.8 Hz, 2H), 5.23 (s, 2H), 3.80 (m, 4H), 3.74 (m, 4H). ^{13}C NMR (101 MHz, DMSO-d_6) δ 167.90, 161.40, 155.22, 154.93, 153.45, 143.43, 143.38, 135.91, 122.28, 118.66, 116.25, 114.31, 111.87, 101.95, 99.32, 48.00, 44.84, 44.84, 44.51. For $C_{21}H_{18}F_2N_6O$, 408.41, found 409.25 $[M + H]^+$. Anal. calcd for $C_{21}H_{18}F_2N_6O$ (%) C, 57.15; H, 4.11; Cl, 16.07; N, 19.04; O, 3.63 found: C, 57.10; H, 4.15; Cl, 16.09; N, 19.01; O, 3.56.

*2-(4-(3-Cyano-1,8-naphthyridin-2-yl)piperazin-1-yl)-N-phenylacetamide (**ANA-1**).* Brown solid; yield (69%), m.p. 149–150 °C. IR (KBr, υ_{max}/cm^{-1}): 3302, 2223, 1673, 1497. ^{1}H NMR (400 MHz, DMSO-d_6) δ 9.84 (s, 1H), 8.95 (s, 1H), 7.65 (dd, J = 8.6, Hz, 2H), 7.32 (dd, J = 10.8, Hz, 4H), 7.06 (d, J = 6.2 Hz, 2H), 3.85–3.79 (m,

4H), 3.24 (s, 2H), 2.78–2.73 (m, 4H). ^{13}C NMR (101 MHz, DMSO-d_6) δ 168.67, 160.83, 157.06, 150.73, 148.92, 139.40, 137.17, 129.35, 124.34, 119.64, 112.06, 61.91, 52.73, 48.51. ESI MS (m/z): calcd. For $C_{21}H_{20}N_6O$, 372.43, found 373.25 $[M + H]^+$. Anal. calcd for $C_{21}H_{20}N_6O$ (%) C, 67.73; H, 5.41; N, 22.57; O, 4.30 found: C, 67.60; H, 5.35; N, 22.64; O, 4.20.

*2-(4-(3-Cyano-1,8-naphthyridin-2-yl)piperazin-1-yl)-N-(4-ethylphenyl)acetamide (**ANA-2**).* Yellow solid; yield (65%), m.p. 153–155 °C. IR (KBr, υ_{max}/cm^{-1}): 3308, 2222, 1672, 1498. ^{1}H NMR (400 MHz, DMSO-d_6) δ 9.73 (s, 1H), 9.00–8.96 (m, 1H), 8.34–8.31 (m, 1H), 7.56 (d, J = 8.5 Hz, 2H), 7.46 (dd, J = 8.0, Hz, 1H), 7.15 (d, J = 8.5 Hz, 4H), 3.81–3.80 (m, 4H), 3.23 (s, 2H), 2.78–2.73 (m, 4H), 2.69–2.65 (q, 2H), 1.16 (t, J = 7.6 Hz, 3H). ^{13}C NMR (101 MHz, DMSO-d_6) δ 168.67, 162.99, 159.58, 156.41, 151.73, 149.20, 146.38, 138.49, 137.54, 131.91, 121.84, 120.85, 117.09, 115.26, 110.78, 61.45, 52.88, 48.94, 36.26, 31.24. ESI MS (m/z): calcd. For $C_{23}H_{24}N_6O$, 400.49, found 423.25 $[M + Na]^+$, Anal. calcd for $C_{23}H_{24}N_6O$ (%) C, 68.98; H, 6.04; N, 20.99; O, 3.99 found: C, 68.94; H, 6.10; N, 20.04; O, 3.90.

*2-(4-(3-Cyano-1,8-naphthyridin-2-yl)piperazin-1-yl)-N-(3,4-dimethylphenyl)acetamide (**ANA-3**).* Brown solid; yield (66%), m.p. 154–155 °C. IR (KBr, υ_{max}/cm^{-1}): 3300, 2228, 1681, 1483. ^{1}H NMR (400 MHz, DMSO-d_6) δ 9.65 (s, 1H), 8.98–8.95 (m, 2H), 8.31 (dd, J = 8.1, Hz, 1H), 7.47 (t, J = 4.0 Hz, 1H), 7.45–7.38 (m, 2H), 7.10–7.04 (m, 2H), 3.83–3.80 (m, 4H), 3.21 (s, 2H), 2.74 (dd, J = 7.5, Hz, 4H), 2.18 (s, 6H). ^{13}C NMR (101 MHz, DMSO-d_6) δ 168.29, 159.31, 156.66, 156.10, 155.30, 153.85, 149.20, 147.86, 138.05, 136.46, 132.45, 131.39, 130.16, 123.47, 121.24, 117.52, 98.88, 61.95, 52.75, 48.54, 20.15, 19.33. ESI MS (m/z): calcd. For $C_{23}H_{24}N_6O$, 400.49, found 423.25 $[M + Na]^+$, Anal. calcd for $C_{23}H_{24}N_6O$ (%) C, 68.98; H, 6.04; N, 20.99; O, 3.99 found: C, 68.93; H, 6.15; N, 20.01; O, 3.97.

*2-(4-(3-Cyano-1,8-naphthyridin-2-yl)piperazin-1-yl)-N-(4-fluorophenyl)acetamide (**ANA-4**).* Brown solid; yield (70%), m.p. 149–151 °C. IR (KBr, υ_{max}/cm^{-1}): 3310, 2215, 1669, 1490. ^{1}H NMR (400 MHz, DMSO-d_6) δ 9.90 (s, 1H), 8.97 (dd, J = 4.4, 2.3 Hz, 1H), 8.31 (dd, J = 8.0, Hz, 1H), 7.71–7.66 (m, 2H), 7.47–7.43 (m, 1H), 7.20–7.13 (m, 2H), 3.84–3.79 (m, 4H), 3.24 (s, 2H), 2.75–2.73 (m, 4H). ^{13}C NMR (101 MHz, DMSO-d_6) δ 168.57, 163.24, 162.72, 160.01, 159.30, 156.85, 149.20, 138.19, 136.70, 135.32, 130.28, 128.38, 124.83, 121.24, 117.61, 116.91, 115.99, 115.42, 61.92, 52.76, 48.50. ESI MS (m/z): calcd. For $C_{21}H_{19}FN_6O$, 390.42, found 389.05 $[M - H]^-$, Anal. calcd for $C_{21}H_{19}FN_6O$ (%) C, 64.60; H, 4.91; F, 4.87; N, 21.53; O, 4.10 found: C, 64.67; H, 4.90; F, 4.90; N, 21.50; O, 4.14.

*N-(4-Bromophenyl)-2-(4-(3-cyano-1,8-naphthyridin-2-yl) piperazin-1-yl)acetamide (**ANA-5**).* Brown solid; yield (62%), m.p. 140–142 °C. IR (KBr, υ_{max}/cm^{-1}): 3251, 2826, 2222, 1673, 1468. ^{1}H NMR (400 MHz, DMSO-d_6) δ 10.00 (s, 1H), 9.00–8.93 (m, 1H), 8.54 (s, 1H), 8.30 (dd, J = 8.0, Hz, 1H), 7.95 (s, 1H), 7.66 (dd, J = 8.9, Hz, 3H), 7.51–7.46 (m, 2H), 3.84–3.77 (m, 4H), 2.89 (s, 2H). 2.89–2.87 (m, 4H). ^{13}C NMR (101 MHz, DMSO-d_6) δ 168.67, 162.99, 159.58, 156.41, 151.73, 149.20, 138.49, 137.54, 131.91, 121.84, 120.85, 117.09, 115.26, 110.78, 61.45, 52.88, 48.94. ESI MS (m/z): calcd. For $C_{21}H_{19}BrN_6O$, 451.33, found 449.00 $[M-H]^-$. Anal. calcd for $C_{21}H_{19}BrN_6O$ (%) C, 55.89; H, 4.24; Br, 17.70; N, 18.62; O, 3.54 found: C, 55.80; H, 4.20; Br, 17.80; N, 18.60; O, 3.56.

*2-(4-(3-Cyano-1,8-naphthyridin-2-yl)piperazin-1-yl)-N-(2-fluorophenyl)acetamide (**ANA-6**).* Brown solid; yield (66%), m.p. 135–136 °C. IR (KBr, υ_{max}/cm^{-1}): 3310, 2221, 1672, 1474. ^{1}H NMR (400 MHz, DMSO-d_6) δ 9.70 (s, 1H), 9.02–8.96 (m, 2H), 8.32 (dd, J = 8.1, Hz, 1H), 7.99–7.95 (m, 1H), 7.46 (dd, J = 8.0, Hz, 1H), 7.21–7.17 (m, 3H), 3.84–3.78 (m, 4H), 3.30 (s, 2H), 2.82–2.77 (m, 4H). ^{13}C NMR (101 MHz, DMSO-d_6) δ 168.66, 162.67, 158.95, 157.05, 155.48, 149.48, 137.54, 126.49, 124.95, 123.41, 120.87, 117.74, 117.42, 116.16, 61.35, 52.39, 48.54. ESI MS (m/z): calcd. For $C_{21}H_{19}FN_6O$, 390.42, found 413.20 $[M + Na]^+$. Anal. calcd for $C_{21}H_{19}FN_6O$ (%) C, 64.60; H, 4.91; F, 4.87; N, 21.53; O, 4.10 found: C, 64.65; H, 4.90; F, 4.80; N, 21.52; O, 4.13.

*2-(4-(3-Cyano-1,8-naphthyridin-2-yl)piperazin-1-yl)-N-(2-nitrophenyl)acetamide (**ANA-7**).* Red solid; yield (56%), m.p. 151–152 °C. IR (KBr, υ_{max}/cm^{-1}): 3253, 2824, 1674, 1459. ^{1}H NMR (400 MHz, DMSO-d_6) δ 11.60 (s, 1H), 9.01–8.96 (m, 2H), 8.62 (dd, J = 8.4, Hz, 1H), 8.32 (dd, J = 8.0, Hz, 1H), 8.20 (dd, J = 8.4, Hz, 1H), 7.81–7.74 (m, 1H), 7.47 (dd, J = 8.0, Hz, 1H), 7.36–7.28 (m, 1H), 3.84–3.82 (m, 4H), 3.32 (s, 1H), 2.87–2.80 (m, 4H). ^{13}C NMR (101 MHz, DMSO-d_6) δ 170.28, 163.36, 159.25, 156.79, 155.50, 146.96, 138.50, 135.37, 134.09, 127.15, 124.31, 122.14, 120.89, 119.93, 118.36, 116.50, 115.80, 113.35, 61.73, 52.94, 48.89. ESI MS (m/z): calcd. For $C_{21}H_{19}N_7O_3$, 417.43, found 418.20 $[M + H]^+$. Anal. calcd for $C_{21}H_{19}N_7O_3$ (%) C, 60.42; H, 4.59; N, 23.49; O, 11.50 found: C, 60.40; H, 4.53; N, 23.44; O, 11.55.

*2-(4-(3-Cyano-1,8-naphthyridin-2-yl)piperazin-1-yl)-N-(3(trifluoromethyl)phenyl)acetamide (**ANA-8**).* Brown solid; yield (61%), m.p. 128–130 °C. IR (KBr, υ_{max}/cm^{-1}): 3252, 2825, 2240, 1681, 1460. ^{1}H NMR (400 MHz, DMSO-d_6) δ 10.19 (s, 1H), 8.96 (m, J = 5.4, Hz, 2H), 8.30 (dd, J = 8.0, Hz, 2H), 8.16 (s, 1H), 7.94 (d, J = 9.1 Hz, 1H), 7.55 (d, J = 8.4 Hz, 2H), 7.46–7.39 (m, 3H), 3.84–3.79 (m, 4H), 3.28 (s, 1H), 2.79–2.71 (m, 4H). ^{13}C NMR (101 MHz, DMSO-d_6) δ 170.27, 163.33, 158.94, 157.34, 155.51, 149.48, 140.66, 137.58, 130.33, 129.33, 123.62, 123.43, 120.87, 119.92, 118.01, 117.12, 116.82, 116.47, 62.09, 52.72, 48.47. ESI MS (m/z): calcd. For $C_{22}H_{19}F_3N_6O$, 440.43, found 463.20 $[M + Na]^+$. Anal. calcd for $C_{22}H_{19}F_3N_6O$ (%) C, 60.00; H, 4.35; F, 12.94; N, 19.08; O, 3.63 found: C, 60.05; H, 4.30; F, 12.90; N, 19.07; O, 3.60.

*2-(4-(3-Cyano-1,8-naphthyridin-2-yl)piperazin-1-yl)-N-(3,4-difluorophenyl)acetamide (**ANA 9**).* Brown solid; yield (64%), m.p. 209–210 °C. IR (KBr, υ_{max}/cm^{-1}): 3199, 2820, 2220, 1679, 1472. ^{1}H NMR (400 MHz, DMSO-d_6) δ 10.05 (s, 1H), 8.99–8.94 (m, 1H), 8.34–8.26 (m, 1H), 8.00 (d, J = 2.6 Hz, 1H), 7.95 (s, 1H), 7.62 (dd, J = 9.0, Hz, 1H), 7.45 (dd, J = 8.0, Hz, 1H), 7.38 (t, J = 9.1 Hz, 2H), 3.85–3.78 (m, 4H), 3.25 (s, 2H), 2.74 (dd, J = 7.7, Hz, 4H). ^{13}C NMR (101 MHz, DMSO-d_6) δ 169.32, 163.33, 162.72, 158.98, 156.78, 155.78, 149.19, 143.53, 138.21, 136.34, 126.52, 122.10, 120.86, 120.28, 119.94, 117.73, 62.71, 61.43, 52.73, 48.46. ESI MS (m/z): calcd. For $C_{21}H_{18}F_2N_6O$, 408.41, found 407.05 $[M-H]^-$. Anal. calcd for $C_{21}H_{18}F_2N_6O$ (%) C, 61.76; H, 4.44; F, 9.30; N, 20.58; O, 3.92 found: C, 61.70; H, 4.40; F, 9.33; N, 20.54; O, 3.90.

*2-(4-(3-Cyano-1,8-naphthyridin-2-yl)piperazin-1-yl)-N-(3-nitrophenyl)acetamide (**ANA-10**).* Brown solid; yield (73%), m.p. 129–130 °C. IR (KBr, υ_{max}/cm^{-1}): 3258, 2824, 2218, 1669, 1473. ^{1}H NMR (400 MHz, DMSO-d_6) δ 10.45 (s, 1H), 8.98–8.95 (m, 1H),

8.72 (t, J = 2.1 Hz, 1H), 8.52 (s, 1H), 8.30 (dd, J = 8.1, Hz, 1H), 8.07–8.02 (m, 1H), 7.98–7.92 (m, 2H), 7.63–7.57 (m, 2H), 7.47–7.43 (m, 1H), 3.84–3.78 (m, 4H), 3.31 (s, 2H), 2.79–2.75 (m, 4H). ^{13}C NMR (101 MHz, DMSO-d_6) δ 169.61, 166.78, 162.70, 159.92, 157.05, 149.44, 148.54, 140.70, 138.52, 134.12, 130.42, 126.54, 121.20, 118.01, 116.81, 114.92, 61.44, 52.38, 48.26. ESI MS (m/z): calcd. For $C_{21}H_{19}N_7O_3$, 417.43, found 416.05 $[M–H]^-$. Anal. calcd for $C_{21}H_{19}N_7O_3$ (%) C, 60.42; H, 4.59; N, 23.49; O, 11.50 found: C, 60.42; H, 4.59; N, 23.49; O, 11.50.

*2-(4-(3-Cyano-1,8-naphthyridin-2-yl)piperazin-1-yl)-N-(4-nitrophenyl)acetamide (**ANA-11**).* Brown solid; yield (67%), m.p. 189–190 °C. IR (KBr, υ_{max}/cm^{-1}): 3250, 2224, 1694, 1449, 1395. ^{1}H NMR (400 MHz, DMSO-d_6) δ 10.47 (s, 1H), 8.99–8.96 (m, 1H), 8.31 (dd, J = 8.0, Hz, 1H), 8.24 (dd, J = 6.8, Hz, 2H), 7.95–7.93 (m, 3H), 7.45 (dd, J = 8.0, 4.4 Hz, 1H), 6.62–6.58 (m, 1H), 3.84–3.79 (m, 4H), 3.34 (s, 2H), 2.80–2.75 (m, 4H). ^{13}C NMR (101 MHz, DMSO-d_6) δ 169.33, 158.99, 157.05, 156.11, 149.45, 147.90, 145.43, 142.87, 141.59, 138.52, 136.96, 130.60, 124.97, 119.33, 116.80, 114.25, 112.39, 62.07, 52.38, 48.49. ESI MS (m/z): calcd. For $C_{21}H_{19}N_7O_3$, 417.43, found 418.20 $[M + H]^+$. Anal. calcd for $C_{21}H_{19}N_7O_3$ (%) C, 60.42; H, 4.59; N, 23.49; O, 11.50 found: C, 60.40; H, 4.57; N, 23.40; O, 11.55.

*2-(4-(5-Nitrofuran-2-carbonyl) piperazin-1-yl)-1,8-naphthyridine-3-carbonitrile (**ANA-12**).* Red solid; yield (69%), m.p. 230–231 °C. IR (KBr, υ_{max}/cm^{-1}): 3240, 2220, 1694, 1570, 1449, 1370. ^{1}H NMR (400 MHz, DMSO-d_6) δ 9.06 (s, 1H), 9.05 (d, J = 2.1 Hz, 1H), 8.39 (dd, J = 8.0, 2.0 Hz, 1H), 7.86 (d, J = 3.9 Hz, 1H), 7.54 (dd, J = 8.0, 4.4 Hz, 1H), 7.41 (d, J = 3.9 Hz, 1H), 3.00 (s, 4H), 2.84 (s, 4H). ^{13}C NMR (101 MHz, DMSO-d_6) δ 164.03, 158.82, 157.14, 149.83, 138.20, 132.62, 131.97, 120.99, 114.05, 113.36, 37.63, 34.65. ESI MS (m/z): calcd. For $C_{18}H_{14}N_6O_4$, 378.11 found 379.10 $[M + H]^+$. Anal. calcd for C, 57.14; H, 3.73; N, 22.21; O, 16.91 found: C, 57.12; H, 3.70; N, 22.24; O, 16.89.

Data availability

Data are available in ESI† section.

Conflicts of interest

There are no conflicts of interest declared by the authors.

Acknowledgements

KVGCS would like to thank the Council for Scientific and Industrial Research (CSIR), New Delhi (F. No. 02(392)/21/EMR II) and the SERB-CRG (CRG/2022/001889), New Delhi for funding the work. Central Analytical Laboratory Facility at BITS Pilani Hyderabad Campus is greatfully acknowledged. KVGCS would like to thank DST-FIST (SR/FST/CS-I/2020/158) at BITS Pilani, Hyderabad Campus for the HRMS facility.

References

1 A. Shinde, *et al.*, Synthesis of 2-(6-substituted quinolin-4-yl)-1-(4-aryl-1H-1, 2, 3-triazol-1-yl) propan-2-ol as potential antifungal and anti-tubercular agents, *Eur. J. Med. Chem. Rep.*, 2023, **7**, 100102.
2 P. P. Thakare, *et al.*, Synthesis and Biological Evaluation of New 1, 2, 3-Triazolyl-Pyrazolyl-Quinoline Derivatives as Potential Antimicrobial Agents, *ChemistrySelect*, 2020, **5**(15), 4722–4727.
3 A. Mabhula and V. Singh, Drug-resistance in *Mycobacterium tuberculosis*: where we stand, *MedChemComm*, 2019, **10**(8), 1342–1360.
4 A. Sharma, *et al.*, A. Tuberculosis: an overview of the immunogenic response, disease progression, and medicinal chemistry efforts in the last decade toward the development of potential drugs for extensively drug-resistant tuberculosis strains, *J. Med. Chem.*, 2021, **64**(8), 4359–4395.
5 S. Tiberi, *et al.*, Tuberculosis: progress and advances in development of new drugs, treatment regimens, and host-directed therapies, *Lancet Infect. Dis.*, 2018, **18**(7), e183–e198.
6 D. S. Reddy, *et al.*, Design, synthesis, molecular docking, and biological evaluation of coumarin-thymidine analogs as potent anti-TB agents, *Arch. Pharm.*, 2023, **56**(5), 2200633.
7 S. G. Mane, *et al.*, Design, synthesis, molecular docking, anti-proliferative and anti-TB studies of 2H-chromen-8-azaspiro [4.5] decane-7, 9-dione conjugates, *J. Mol. Struct.*, 2021, **1227**, 129530.
8 A. Sinha, *et al.*, ON donor tethered copper (II) and vanadium (V) complexes as efficacious anti-TB and anti-fungal agents with spectroscopic approached HSA interactions, *Heliyon*, 2022, **8**(8), e10105.
9 J. B. Araújo-Neto, *et al.*, Enhancement of antibiotic activity by 1, 8-naphthyridine derivatives against multi-resistant bacterial strains, *Molecules*, 2021, **26**(23), 7400.
10 A. N. Al-Romaizan, *et al.*, Novel 1, 8-naphthyridine derivatives: design, synthesis and *in vitro* screening of their cytotoxic activity against MCF7 cell line, *Open Chem.*, 2019, **17**(1), 943–954.
11 A. P. Taylor, *et al.*, Modern advances in heterocyclic chemistry in drug discovery, *Org. Biomol. Chem.*, 2016, **14**(28), 6611–6637.
12 P. M. Sivakumar and G. Iyer, QSAR studies on substituted 3- or 4-phenyl-1, 8-naphthyridine derivatives as antimicrobial agents, *Med. Chem. Res.*, 2012, 788–795.
13 A. K. Parhi, *et al.*, Anti-bacterial activity of quinoxalines, quinazolines, and 1, 5-naphthyridines, *Bioorg. Med. Chem. Lett.*, 2013, **23**(17), 4968–4974.
14 E. P. Garvey, *et al.*, The naphthyridinone GSK364735 is a novel, potent human immunodeficiency virus type 1 integrase inhibitor and antiretroviral, *Lancet Infect. Dis.*, 2008, **2**(3), 901–908.
15 V. Kumar, *et al.*, 1, 8-Naphthyridine-3-carboxamide derivatives with anticancer and anti-inflammatory activity, *Eur. J. Med. Chem.*, 2009, **44**(8), 3356–3362.
16 L. S. Zhuo, *et al.*, 2, 7-naphthyridinone-based MET kinase inhibitors: A promising novel scaffold for antitumor drug development, *Eur. J. Med. Chem.*, 2019, **178**, 705–714.
17 A. Garg and A. Tadesse, A four-component domino reaction: an eco-compatible and highly efficient construction of 1, 8-

naphthyridine derivatives, there *in silico* molecular docking, drug likeness, ADME, and toxicity studies, *J. Chem.*, 2021, **2021**, 1–6.

18 R. A. Kardile, *et al.*, Design and synthesis of novel conformationally constrained 7, 12-dihydrodibenzo [*b*, *h*][1, 6] naphthyridine and 7H-Chromeno [3, 2-*c*] quinoline derivatives as topoisomerase I inhibitors: *In vitro* screening, molecular docking and ADME predictions, *Bioorg. Chem.*, 2021, **115**, 105174.

19 M. Badawneh, *et al.*, Synthesis of variously substituted 1, 8-naphthyridine derivatives and evaluation of their anti-mycobacterial activity, *Il Farmaco*, 2002, **57**(8), 631–639.

20 M. Dinakaran, *et al.*, Anti-tubercular activities of novel benzothiazolo naphthyridone carboxylic acid derivatives endowed with high activity toward multi-drug resistant tuberculosis, *Biomed. Pharmacother.*, 2009, **63**(1), 11–18.

21 M. Badawneh, *et al.*, Synthesis of 3-or 4-phenyl-1, 8-naphthyridine derivatives and evaluation of anti-mycobacterial and antimicrobial activity, *Il Farmaco*, 2003, **58**(9), 859–866.

22 M. Badawneh and J. Aljamal, Synthesis and anti-tubercular activity of piperidine and morpholine 1, 8 naphthyridine analogues, *Int. J. Pharmacol. Pharm. Sci.*, 2016, **8**(12), 252–257.

23 X. Wang and Y. Wang, Nitrile-containing pharmaceuticals: target, mechanism of action, and their SAR studies, *RSC Med. Chem.*, 2021, **12**(10), 1650–1671.

24 X. Wang, *et al.*, Nitrile-containing pharmaceuticals: target, mechanism of action, and their SAR studies, *RSC Med. Chem.*, 2021, **12**(10), 1650–1671.

25 A. Wissner, *et al.*, Syntheses and EGFR kinase inhibitory activity of 6-substituted-4-anilino [1, 7] and [1, 8] naphthyridine-3-carbonitriles, *Bioorg. Med. Chem. Lett.*, 2004, **14**(6), 1411–1416.

26 R. Mahesh, *et al.*, Potential antidepressants: Pharmacology of 2-(4-methyl piperazin-1-yl)-1, 8-naphthyridine-3-carbonitrile in rodent behavioural models, *Int. J. Pharm. Sci.*, 2007, **62**(12), 919–924.

27 R. Mahesh, *et al.*, Microwave assisted synthesis of 2-(4-substituted piperazin-1-yl)-1, 8-naphthyridine-3-carbonitrile as a new class of serotonin 5-HT3 receptor antagonists, *Bioorg. Med. Chem. Lett.*, 2004, **14**(20), 5179–5181.

28 S. G. Nayak, *et al.*, Novel thiazolidin-4-one clubbed thiophene derivatives *via* Gewald synthesis as anti-tubercular and anti-inflammatory agents, *J. Chin. Chem. Soc.*, 2021, (6), 1116–1127.

29 Y. Q. Hu, *et al.*, Isoniazid derivatives and their anti-tubercular activity, *Eur. J. Med. Chem.*, 2017, **133**, 255–267.

30 P. S. Girase, *et al.*, An appraisal of anti-mycobacterial activity with structure-activity relationship of piperazine and its analogues: A review, *Eur. J. Med. Chem.*, 2021, **210**, 112967.

31 S. Konduri, *et al.*, Design and synthesis of purine connected piperazine derivatives as novel inhibitors of *Mycobacterium tuberculosis*, *Bioorg. Med. Chem. Lett.*, 2020, **30**(22), 127512.

32 A. Wang, *et al.*, Design, synthesis and biological activity of N-(amino) piperazine-containing benzothiazinones against *Mycobacterium tuberculosis*, *Eur. J. Med. Chem.*, 2021, **218**, 113398.

33 K. Gnanavelu, K. S. V. K. Eswaran and S. Karthikeyan, Novel quinoline-piperazine hybrids: the design, synthesis and evaluation of anti-bacterial and anti-tuberculosis properties, *RSC Med. Chem.*, 2023, **14**(1), 183–189.

34 X. Qin, *et al.*, Design, synthesis and anti-TB and anti-bacterial activity of Ciprofloxacin derivatives containing N-(amino) piperazine moieties, *Med. Chem. Res.*, 2023, **2**(3), 556–570.

35 D. Nawrot, *et al.*, N-pyridinylbenzamides: an isosteric approach towards new anti-mycobacterial compounds, *Chem. Biol. Drug Des.*, 2021, **7**(3), 686–700.

36 S. Srinivasarao, *et al.*, Seeking potent anti-tubercular agents: design and synthesis of substituted-N-(6-(4-(pyrazine-2-carbonyl) piperazine/homopiperazine-1-yl) pyridin-3-yl) benzamide derivatives as anti-tubercular agents, *RSC Adv.*, 2020, **10**(21), 12272–12288.

37 B. C. Giacobbo, *et al.*, New insights into the SAR and drug combination synergy of 2-(quinolin-4-yloxy) acetamides against *Mycobacterium tuberculosis*, *Eur. J. Med. Chem.*, 2017, **126**, 491–501.

38 H. Wang, *et al.*, Design, synthesis and anti-mycobacterial activity of novel nitrobenzamide derivatives, *Chin. Chem. Lett.*, 2019, **30**(2), 413–416.

39 K. V. Gowri Chandra Sekhar, *et al.*, Design, synthesis, and preliminary *in vitro* and *in vivo* pharmacological evaluation of 2- {4-[4-(2, 5-disubstituted thiazol-4-yl) phenylethyl] piperazin-1-yl}-1, 8-naphthyridine-3-carbonitriles as atypical antipsychotic agents, *J. Enzyme Inhib. Med. Chem.*, 2011, **26**(4), 561–568.

40 Y. M. Khetmalis, *et al.*, Design, synthesis and biological evaluation of novel oxindole analogs as anti-tubercular agents, *Future Med. Chem.*, 2023, **15**(15), 1323–1342.

41 A. Daina, *et al.*, SwissADME: a free web tool to evaluate pharmacokinetics, drug-likeness and medicinal chemistry friendliness of small molecules, *Sci. Rep.*, 2021, **7**, 42717.

42 M. S. Prasad, *et al.*, Mycobacterium enoyl acyl carrier protein reductase (InhA): A key target for anti-tubercular drug discovery, *Bioorg. Chem.*, 2021, **115**, 105242.

43 G. S. Pedgaonkar, *et al.*, Development of 2-(4-oxoquinazolin-3 (4H)-yl) acetamide derivatives as novel enoyl-acyl carrier protein reductase (InhA) inhibitors for the treatment of tuberculosis, *Eur. J. Med. Chem.*, 2014, **86**, 613–627.

44 S. İ. Dingiş Birgül, *et al.*, *In silico* design, synthesis and anti-tubercular activity of novel 2-acylhydrazono-5-arylmethylene-4-thiazolidinones as enoyl-acyl carrier protein reductase inhibitors, *J. Biomol. Struct. Dyn.*, 2024, **16**, 1–9.

45 Y. M. Khetmalis, *et al.*, Design, synthesis and anti-mycobacterial evaluation of imidazo [1, 2-*a*] pyridine analogues, *RSC Med. Chem.*, 2022, **13**(3), 327–342.

46 S. Satisha and V. G. Revanasiddappa, Anti-mycobacterial, Molecular Docking and ADME Studies of Spiro Naphthyridine Pyrimidine and N-(Quinolin-8-yl) acetamide Derivatives, *ChemistrySelect*, 2023, **8**(28), e202301047.